

See discussions, stats, and author profiles for this publication at: <http://www.researchgate.net/publication/272309921>

Development of thermal boundary condition model at metal/die interface of high pressure die casting process

ARTICLE *in* INTERNATIONAL JOURNAL OF CAST METALS RESEARCH · AUGUST 2011

Impact Factor: 0.48 · DOI: 10.1179/136404611X13001912813825

CITATION

1

READS

21

5 AUTHORS, INCLUDING:



Zhipeng Guo

Tsinghua University

28 PUBLICATIONS 71 CITATIONS

SEE PROFILE



Shoumei Xiong

Tsinghua University

70 PUBLICATIONS 247 CITATIONS

SEE PROFILE



Baicheng Liu

Tsinghua University

126 PUBLICATIONS 372 CITATIONS

SEE PROFILE

Development of thermal boundary condition model at metal/die interface of high pressure die casting process

Z.-P. Guo¹, S.-M. Xiong*¹, B. C. Liu¹, M. Li² and J. Allison²

A thermal boundary condition model at the metal/die interface of a high pressure die casting process was developed based on two important correlations. The first is the relationship between the maximum interfacial heat transfer coefficient (IHTC) and the initial die surface temperature, and the other is between the IHTC and the casting solid fraction. The IHTC at the metal/die interface during solidification of high pressure die casting process can be divided into four stages, namely, the initial increasing stage, higher value maintaining stage, fast decreasing stage and lower value stage. By applying the regression method, it was found that the maximum heat transfer coefficient during the initial increasing stage changes as a function of the initial die surface temperature, and during the fast decreasing stage, the heat transfer coefficient changes as a function of the casting solid fraction.

Keywords: High pressure die casting, Interfacial heat transfer coefficient, Boundary condition, Solidification

This paper is part of a special issue of papers selected from MCSP8, the 8th Pacific Rim Conference on Modeling of Casting and Solidification Processes

Introduction

High pressure die casting (HPDC) is a net shape process for producing thin wall components for the manufacturing industry. During the process, the solidification of castings is highly dependent on the heat transfer behaviour at the metal/die interface, and it is believed that such heat transfer behaviour could directly influence the formation of the microstructure and defects and the final mechanical properties of the castings. Interfacial heat transfer coefficient is a key parameter characterizing the heat transfer behaviour at the metal/die interface, and the determination and application of this coefficient is becoming a key issue to the researchers nowadays.

Studies concerning the metal/die interfacial heat transfer during the HPDC process have been performed since the 1970s,^{1,2} but it is not until recently that these investigations have attracted much attention. The influence of the applied pressure on the heat transfer coefficient is one of the most hotly investigated topics within this area. It is well established that the application of a high pressure could greatly enhance the heat transfer at the metal/die interface.³ However, with a further increase in the applied pressure, as concluded by Papai and Mobley,⁴ the thermal field and the heat flux to the die could be hardly changed. Similar results were observed by El-Mahallawy *et al.*,⁵ Dour *et al.*⁶ and Hamasaiid *et al.*⁷

However, Sekhar *et al.*⁸ found that by casting the Al–Si alloy against an H-13 steel die using a pressurised apparatus, the influence of the pressure on the heat transfer could still be prominent even under a very high pressure situation. Guo *et al.*⁹ conducted an HPDC experiment using a ‘step shape’ casting. They found that the influence of the pressure could only be prominent if the casting step is sufficiently thick; for the thinner steps, however, such influence can be neglected.

The fast shot velocity and the initial die temperature were also found to have great influences on the heat transfer during the HPDC process. According to Dour *et al.*,⁶ a higher velocity always leads to a higher heat transfer coefficient and heat flux. This trend was also observed by Guo *et al.*¹⁰ and Hamasaiid *et al.*¹¹ They believed that this effect is mainly caused by the in cavity pressure arising from the impact of the melt to the die surface. Furthermore, Papai and Mobley⁴ and Dour *et al.*⁶ found that the peak value of heat flux or heat transfer coefficient decreases as the initial die temperature increases. However, according to Guo *et al.*,¹⁰ this trend is only prominent at thicker parts of the casting.

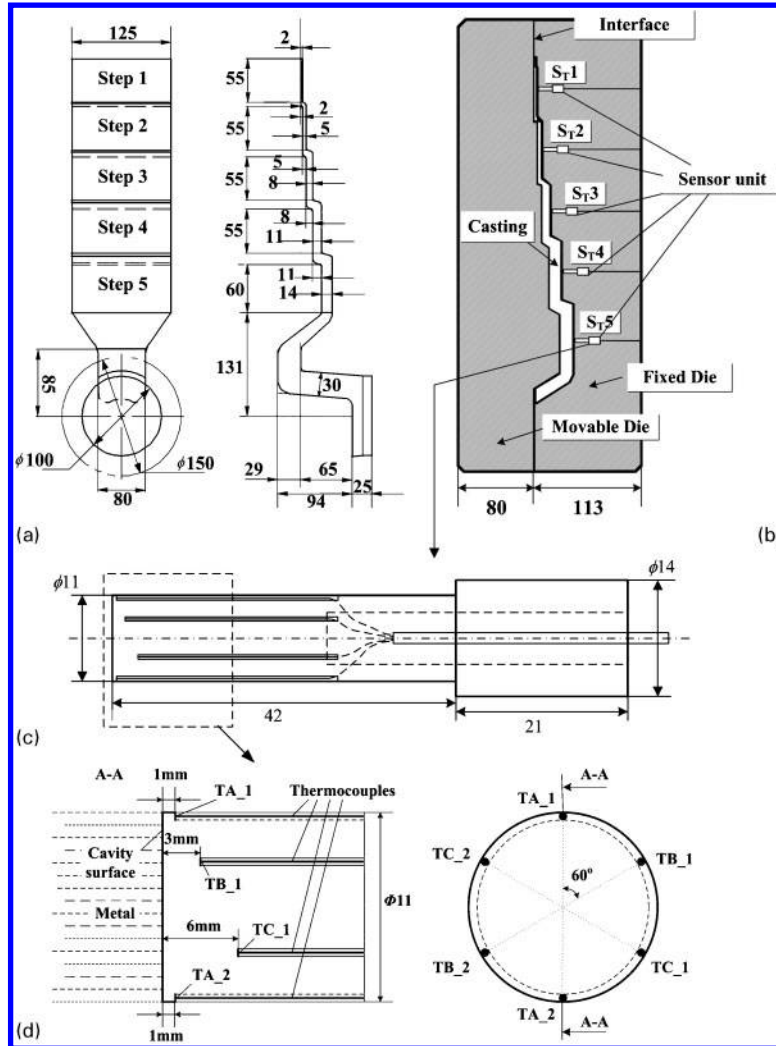
Whereas many processing parameters during HPDC were found to have an influence on the heat transfer coefficient, the relative contribution of each factor is not quantitatively known. In addition, the dependence of the solidification status on the heat transfer has not been thoroughly investigated and thus is not well understood. This greatly restricts the application of the transient heat transfer coefficient in practice, i.e. evaluation of the three-dimensional thermal field during HPDC.

As such, the primary objectives of the present study are:

¹State Key Laboratory of Automotive Safety and Energy, Department of Mechanical Engineering, Tsinghua University, Beijing 100084, China

²Research and Advanced Engineering Department, Scientific Research Laboratory, Ford Motor Company, Dearborn, MI 48121, USA

*Corresponding author, email smxiong@tsinghua.edu.cn



1 Graphical illustration of a 'step shape' casting, b installation of temperature sensor units inside die, c configuration of sensor unit and d adjustment of thermocouples inside sensor unit

- (i) to quantitatively evaluate the influence of the processing parameters on the heat transfer coefficient
- (ii) to investigate the relationship among casting solid fraction, casting solidifying rate and heat transfer coefficient
- (iii) to develop a model capable of accurately simulating the thermal boundary conditions during the HPDC process.

Experimental

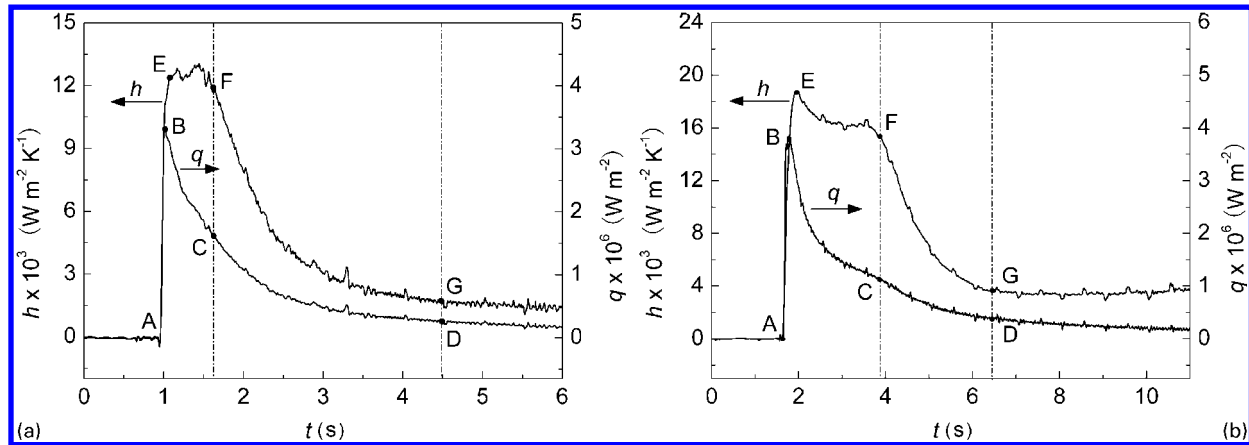
The heat transfer coefficient was determined using the following experimental procedure. This has been described in detail in Ref. 10 but is also briefly given here.

Table 1 Thermal property of related materials

Thermal properties	AM50	ADC12	H-13
Thermal conductivity/ W m ⁻² K ⁻¹	62	92	31.2–0.0137*
Specific heat/J kg ⁻¹ K ⁻¹	1050	963	478–0.219T
Density/kg m ⁻³	1780	2700	7730–0.24T
Solidus temperature/°C	546	531	1404
Liquidus temperature/°C	628	587	1471
Latent heat/J kg ⁻¹	373 000	389 000	209 350

*T is temperature (°C).

Two commercial alloys, namely, AM50 and ADC12, were cast against an H-13 steel die on a TOYO 650 t cold chamber die casting machine. The thermal properties of these materials are summarised in Table 1.⁹ The 'step shape' casting used during the experiment, as shown in Fig. 1a, had five different thicknesses from 2 mm (step 1) to 14 mm (step 5), with an interval of 3 mm. Inside the die corresponding to each step, temperatures at 1, 3 and 6 mm from the interface were measured using a specially designed temperature sensor unit. As shown in Fig. 1b, five sensor units (indicated by S_T1–S_T5) were installed inside the die. Each sensor unit was installed until the front wall of the sensor unit approached the cavity surface. The configuration of the sensor unit is shown in Fig. 1c and d. On each sensor unit, six 0.8 mm wide and 1 mm deep grooves were machined for the placement of the thermocouples. At the end of each groove, the thermocouple was welded in order to maintain better contact with the sensor unit. The thermocouples were sheathed K type thermocouples with a wire diameter of only 0.1 mm. The temperature sensor unit was made using the same material as the die, i.e. H-13 steel, to ensure that the thermal field would not be distorted. The temperature was measured by a data acquisition system manufactured by Integrated Measurement and Control Corporation (IMC) with a sampling rate of 200 Hz.



2 Inversely determined heat transfer coefficient and heat flux at step 3 of a AM50 and b ADC12 alloys

Experiments were performed under different operation conditions. The influences of the casting pressure (24–67 MPa), fast shot velocity ($0.7\text{--}4\text{ m s}^{-1}$), slow shot velocity ($0.2\text{--}0.8\text{ m s}^{-1}$), pressure intensification time (40–100 ms), melt pouring temperature (640–710°C) and die temperature (90–180°C) were considered. For each casting condition, die casting cycles were repeated until the thermal equilibrium inside the die was achieved. A total of ~ 300 shots were performed for each alloy.

Results and discussion

The heat transfer coefficient was determined by applying the temperature measurements into a self-developed inverse thermal programme based on the sequential estimation method introduced by Beck *et al.*¹² Details of the mathematical model can be found in Ref. 10. During the determination, the following assumptions were made:

- (i) the heat transfer at each step is one-dimensional
- (ii) the step centre is adiabatic
- (iii) the initial temperature of the casting is equal to the melt temperature.

Evolution of heat transfer coefficient

Figure 2 shows the determined heat transfer coefficient and associated heat flux at step 3 for both AM50 and ADC12 alloys. Experiments were conducted with a casting pressure of 67 MPa, a fast shot velocity of 4 m s^{-1} , a slow shot velocity of 0.2 m s^{-1} , a pressure intensification time of 40 ms and a melt temperature of 680°C.

As shown in Fig. 2a, the heat flux (represented by curve q) for the AM50 alloy shows a classical two stage change: increasing abruptly first and declining continuously afterwards. The heat transfer coefficient, indicated by curve h , also increases rapidly first. After the heat transfer coefficient reaches E, a plateau follows instead of a continuous decrease. This is probably due to the fact that a tangible shell of metal at the interface had not formed, so that a closer contact between metal and die could be maintained due to the high pressure applied during HPDC. After F, the heat transfer coefficient drops rapidly, indicating that the casting starts to pull back from the die surface due to the casting shrinkage during solidification. This fast decrease in the heat transfer coefficient continues until the casting has totally solidified, as indicated by G.

The foregoing analysis indicates that the evolution of the heat transfer coefficient can be divided into four

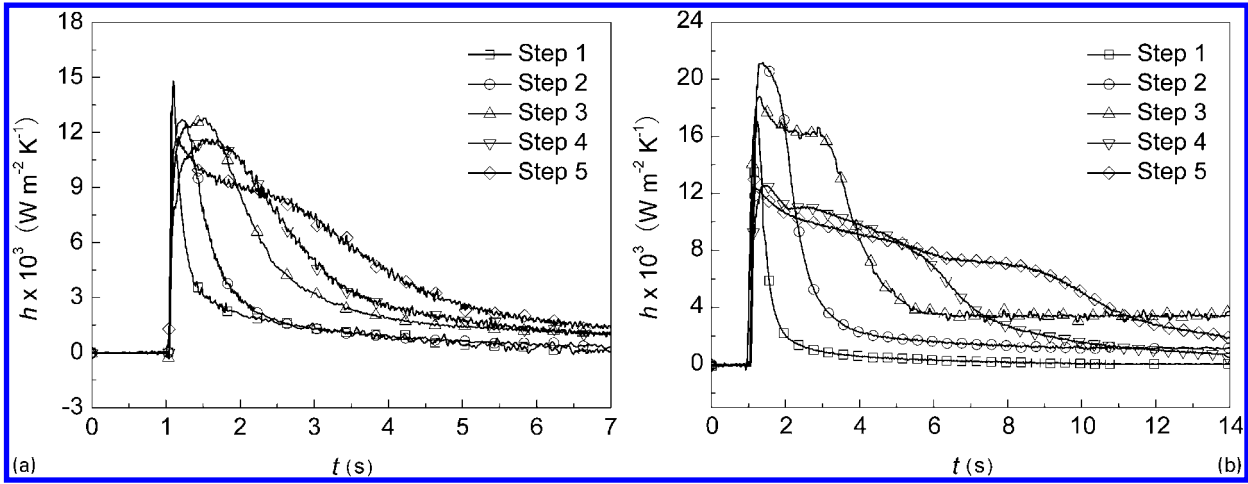
stages, namely, the initial increasing stage, higher value maintaining stage, fast decreasing stage and lower value stage, as indicated in Fig. 2 by AE, EF, FG and after G respectively. For convenience, the Roman numerals I, II, III and IV are used to represent the four different stages for the heat transfer coefficient in the remaining text.

Figure 3 shows the heat transfer coefficient at steps 1–5 for both alloys. Similar to the results at step 3, characteristic points such as E, F and G that mark the different stages of the heat transfer coefficient at other steps can be easily observed. It is notable that it takes more time for the heat transfer coefficient to reach point F as the thickness of the step increases. This is expected, as during the solidification, a thicker step means that a longer close contact status could be maintained between the casting and the die because of a long solidification time and pressure transfer from the casting centre, which results in a longer stage II of the heat transfer coefficient. Moreover, for a particular step, the magnitude of the heat transfer coefficient and the duration of stage II are higher (or longer) for the ADC12 alloy than for the AM50 alloy. The difference in the wetting mechanism during the initial contact and the difference in the magnitude of the latent heat for the two alloys are responsible for this.

Correlation between processing parameters and heat transfer coefficient

As shown in Fig. 2, the first stage of the heat transfer coefficient, i.e. stage I, can be characterised by the maximum value of the heat transfer coefficient h_{\max} . Since the time span for stage I is relatively small (typically 0.1 s) compared with those of other stages, and also due to the fact that a closer contact at the interface could be maintained if the temperature of the casting is higher than the liquidus, it is reasonable to assume that before solidification takes place, the heat transfer coefficient is equal to the maximum heat transfer coefficient.

According to the previous work of the current authors,^{9,10} in addition to the influence of the alloy composition and step thickness, the maximum heat transfer coefficient is mainly affected by the processing parameters. Moreover, it was found that an increase in the fast shot velocity could greatly enhance the maximum heat transfer coefficient at steps 1 and 2. As the step thickness increases, the influence of the initial die surface temperature T_{DI} becomes more prominent, particularly at steps 3–5. In order to get a clear understanding of this influence, let



3 Heat transfer coefficient profiles at steps 1–5 of a AM50 and b ADC12 alloys

$$\eta_h = \frac{h_{max}}{T_{DI}^2} \tag{1}$$

Figure 4 shows the change of η_h versus T_{DI} at steps 1–5 under all the operation conditions. By applying the regression method, it was found that η_h changes as a function of T_{DI} in the manner of

$$\ln \eta_h = \beta_h \ln T_{DI} + \gamma_h \tag{2}$$

where γ_h and β_h are fitted parameters. Combining equations (1) and (2) yields

$$h_{max} = T_{DI}^{2+\beta_h} \exp(x_h) \tag{3}$$

For the ADC12 alloy, as shown in Fig. 4b, an evident increase in the curve slope β_h occurs when T_{DI} exceeds $\sim 260^\circ\text{C}$. After the transition, η_h drops at a much faster rate. For convenience, S1 and S2 are used to represent the change before and after the transition. According to equation (3), the same positive value of $2+\beta_h$ for S1 (0.18) for the two alloys illustrates that the fitted lines are parallel. Moreover, during this period, h_{max} increases as T_{DI} increases, which agrees with the findings of other researchers.^{13–15} After the transition from S1 to S2, the

variable $2+\beta_h$ changes into a negative value of -3.32 , suggesting that h_{max} drops if T_{DI} further increases. However, this transition could not be clearly observed in the results of the AM50 alloy, as shown in Fig. 4a.

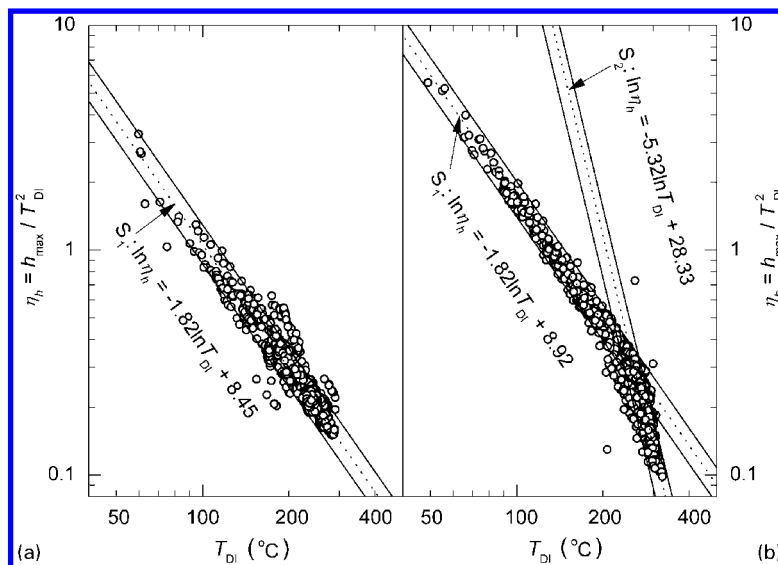
The influence of the processing parameters on the maximum heat flux q_{max} is also of great interest to researchers^{4,6,11} as a similar relationship between q_{max} and T_{DI} could be found as that of h_{max}

$$\eta_q = \frac{q_{max}}{T_{DI}^2} \tag{4a}$$

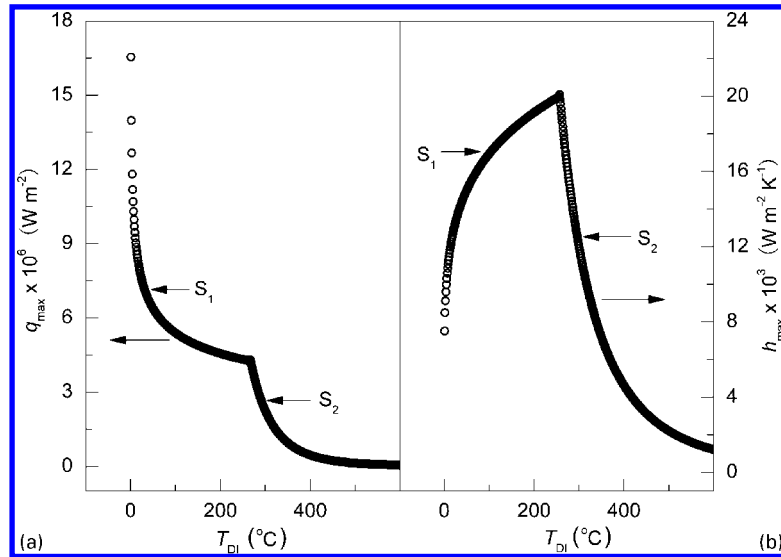
$$\ln \eta_q = \beta_q \ln T_{DI} + \gamma_q \tag{4b}$$

$$q_{max} = T_{DI}^{2+\beta_q} \exp(x_q) \tag{4c}$$

However, for the ADC12 alloy, careful examination of the value $2+\beta_q$ could enable us to find that even after the transition from S1 to S2, q_{max} still drops instead of further increasing, which is different from the heat transfer coefficient. This difference can be clearly observed in Fig. 5a. The transition temperature T_{DI} for q_{max} is $\sim 250^\circ\text{C}$, which is almost the same as that for h_{max} (260°C). The continuous decrease in q_{max} as a function of



4 Graphical illustration of maximum heat transfer coefficient changing with initial die surface temperature and fitted curves according to equation (2) for a AM50 and b ADC12 alloys



5 Graphical illustration of a maximum heat flux and b maximum heat transfer coefficient changing as function of initial die surface temperature according to equations (4c) and (3) for ADC12 alloy

T_{DI} agrees with the results reported in other works.^{4,6,16} The decrease in h_{max} as a function of T_{DI} during the second part of the change, i.e. S2, is also consistent with the results of Dour *et al.*⁶ One of the possible reasons for the absence of the transition for the AM50 alloy, as shown in Fig. 4a, is that during the experiment of the AM50 alloy, the initial die temperature was not high enough to cause the transition. It is therefore believed that if the initial die temperature could be further raised, then the transition could ultimately happen.

Compared with the influences of the fast shot velocity (only prominent at steps 1 and 2) and the casting pressure (only prominent at step 5 for the AM50 alloy),¹⁰ the fact that all the maximum heat transfer coefficients at steps 1–5 change in accordance to equation (2) indicates that the influence of the initial die surface temperature on the heat transfer coefficient is dominant.

Correlation between casting solid fraction and heat transfer coefficient

During stage III, it was found that the heat transfer coefficient can be best fitted using the following equation

$$h = h_0 + A_h \exp(k_h t) \tag{5}$$

where h_0 is a constant value, and A_h and k_h are the

coefficients for the fitted function based on the results shown in Fig. 6.

Figure 6 shows the h profiles and related fitted curves at step 3 for both alloys. It was also found that during stage III, the solid fraction of each step, namely, f_s , can also be fitted using a similar equation

$$f_s = f_0 + A_{fs} \exp(k_{fs} t) \tag{6}$$

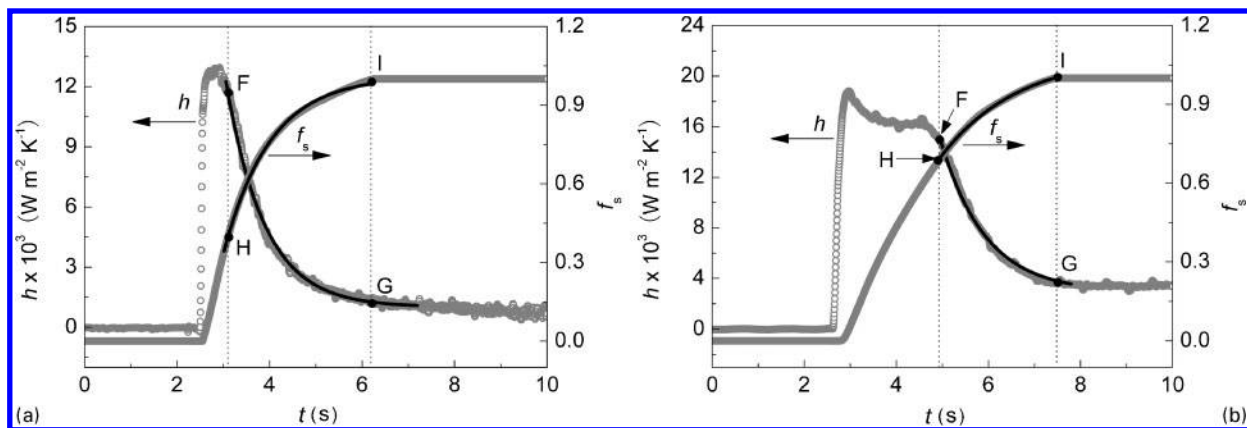
where f_0 is a constant value, A_{fs} and k_{fs} are coefficients for the fitted function based on the results shown in Fig. 7.

Let $\theta_h = h - h_0$ and $\theta_{fs} = f_s - f_0$. According to equations (5) and (6), it can be found that

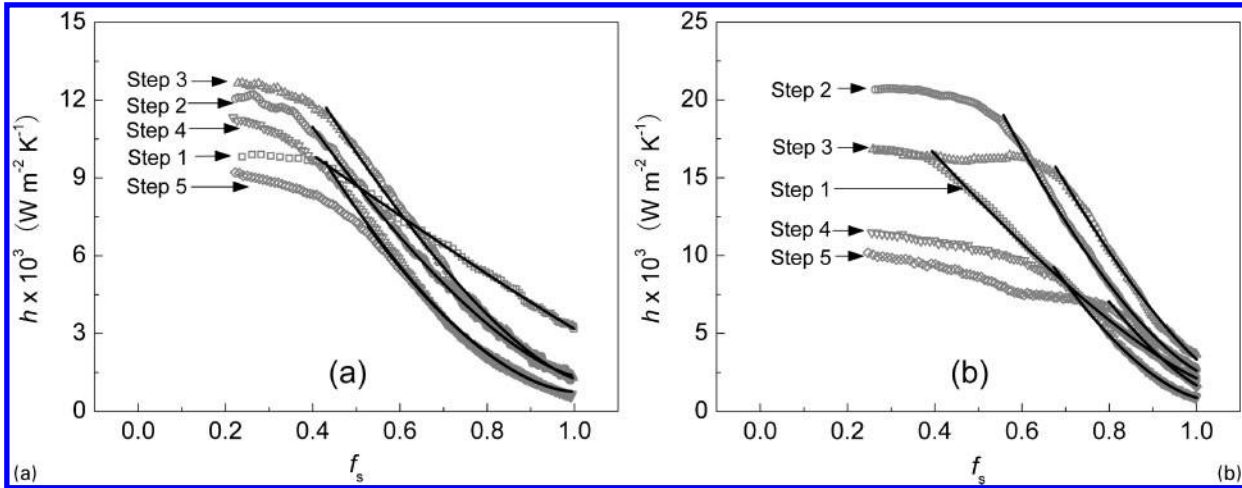
$$\frac{d\theta_h}{dt} = k_h \theta_h \tag{7}$$

$$\frac{d\theta_{fs}}{dt} = k_{fs} \theta_{fs} \tag{8}$$

Equation (7) shows that during stage III, the decreasing rate of the heat transfer coefficient is proportional to its relative magnitude, which means that during this stage, the higher the heat transfer coefficient, the faster it drops. Furthermore, in equation (5), the term h_0 represents the value of the heat transfer coefficient after the metal has totally solidified.



6 Graphical illustration showing inversely determined heat transfer coefficient and fitted curves according to equations (5) and (6) for a AM50 and b ADC12 alloys



7 Graphical illustration showing inversely determined heat transfer coefficient h as function of casting solid fraction f_s during stage III and fitted curves according to equation (13) for a) AM50 and b) ADC12 alloys

Substitution of equation (7) into equation (8) yields

$$\frac{d\theta_h}{\theta_h} = \varepsilon \frac{df_s}{\theta_{fs}} \tag{9}$$

where $\varepsilon = k_h/k_{fs}$. According to equation (9)

$$\theta_h = k_{h-fs}(-\theta_{fs})^\varepsilon \tag{10}$$

which can also be written as

$$h = h_0 + k_{h-fs} \times (f_{s0} - f_s)^\varepsilon \tag{11}$$

where according to equations (5) and (6) k_{h-fs} can be determined by

$$k_{h-fs} = A_h \times (-A_{fs})^{-\varepsilon} \tag{12}$$

Equation (11) provides an explicit and quantitative form interpreting how the heat transfer coefficient changes as the solidification proceeds. Let both sides of equation (11) be divided by h_{max}

$$h = \left[\frac{h_0}{h_{max}} + \frac{k_{h-fs}}{h_{max}} \times (f_{s0} - f_s)^\varepsilon \right] h_{max} \tag{13}$$

By applying these parameters determined by the regression method, Fig. 7 shows a related graphical representation of equation (13) for steps 1–5. Equation (13) provides an excellent fit for the heat transfer coefficient and the casting solid fraction. As expected, the magnitude of k_h decreases as the step thickness increases, indicating that the dropping rate of the heat transfer coefficient at stage III decreases as the step becomes thicker. It is also found that the heat transfer coefficient h_0 after the step totally solidified drops to ~10% of the magnitude of h_{max} , and in most cases, the value of f_{s0} is nearly 1.0, which is expected since this value indicates the end of the solidification.

According to Fig. 7, the decrease in the heat transfer coefficient when $f_s < f_{sF}$ (solid fraction when stage III starts) is much slower compared to that when $f_s > f_{sF}$. It is therefore reasonable to assume a linear change of the heat transfer coefficient during stage II

$$h = h_{max} + \frac{h_{max} - h_F}{f_{sc} - f_{sF}} (f_s - f_{sc}) \tag{14}$$

where h_F is the heat transfer coefficient when $f_s = f_{sF}$, and f_{sc} is the solid fraction when the heat transfer coefficient reaches its maximum, which could be reasonably assumed to be h_0 .

Conclusions

The heat transfer coefficient at the metal/die interface during the HPDC process was determined. The influence of various processing parameters, particularly the initial die surface temperature, on the heat transfer was investigated. Additionally, by investigating the variation in the heat transfer coefficient at different steps, the dependence of the heat transfer coefficient on the casting solid fraction was evaluated and quantified. Moreover, a relationship between the casting solidifying rate and the heat transfer coefficient was determined. From the results of this study, the following conclusions can be drawn.

1. During the solidification process of the HPDC, the heat transfer coefficient can be divided into four stages, namely, the initial increasing stage, the higher value maintaining stage, the fast decreasing stage and the lower value stage.

2. Of all the processing parameters, the initial die surface temperature T_{DI} has the most dominant influence on the heat transfer coefficient, and this influence is mainly focused on the maximum value h_{max} . By applying the regression method, it was found that h_{max} changes as a function of T_{DI} as

$$h_{max} = T_{DI}^{2+\beta_h} \exp(x_h)$$

According to this equation and due to the same positive exponent for the two alloys, the maximum heat transfer coefficient increases as the initial die surface temperature increases. For the ADC12 alloy, however, h_{max} would drop if the initial die surface temperature further increased.

3. During the fast decreasing stage, the dependence of the heat transfer coefficient h on the casting solid fraction f_s can be excellently correlated by the equation

$$h = h_0 + k_{h-fs}(f_{s0} - f_s)^\varepsilon$$

where k_{h-fs} and ε are the parameters related to the step thickness, and h_0 indicates the magnitude of the heat transfer coefficient after the casting is totally solidified.

4. The four stages of the heat transfer coefficient can be characterised by the following equations

- (i) $h = h_{max}$, before and during the initial increasing stage

- (ii) $h = h_{\max} + (f_s/f_{sF})(h_{\max} - h_F)$, higher value maintaining stage
- (iii) $h = h_0 + k_{h-fs}(f_{s0} - f_s)^e$, fast decreasing stage
- (iv) $h = h_0$, lower value stage.

These four equations can therefore be used to simulate the thermal boundary conditions for solidification during the HPDC process.

Acknowledgements

This research was financially supported by the National Science Foundation of China (grant no. 50675114), the National High Technology Research and Development Program of China (grant no. 2009AA03Z114) and the Significant Program on High-end CNC Machine Tool and Base Manufacturing Equipment of China (grant no. 2009ZX04014-082). The experimental work was conducted at Tsinghua-TOYO R&D Centre of Magnesium and Aluminium Alloys Processing Technology with the help of engineers from TOYO Machinery & Metal Co., Ltd.

References

1. C. W. Nelson: Proc. 6th SDCE Int. Die Casting Cong., 1–8; 1970, Cleveland, OH, SDCE.
2. S. Hong, D. G. Backman and R. Mehrabian: *Metall. Mater. Trans. B*, 1979, **10B**, 299–301.
3. S. D. E. Ramati, G. J. Abbaschian, D. G. Backman and R. Mehrabian: *Metall. Mater. Trans. B*, 1978, **9B**, 279–286.
4. J. Papai and C. Mobley: Proc. 16th NADCA Cong. Exp., 377–384; 1991, Detroit, MI, NADCA.
5. N. A. El-Mahallawy, M. A. Taha, E. Pokora and F. Klein: *J. Mater. Process. Technol.*, 1998, **73**, 125–138.
6. G. Dour, M. Dargusch, C. Davidson and A. Nef: *J. Mater. Process. Technol.*, 2005, **169**, 223–233.
7. A. Hamasaiid, G. Dour, M. Dargusch, T. Loulou, C. Davidson and G. Savage: Proc. 11th Conf. on 'Modeling of casting, welding and advanced solidification processes', (ed. C.-A. Gandin and M. Bellet), 1205–1212; 2006, Warrendale, PA, TMS.
8. J. A. Sekhar, G. J. Abbaschian and R. Mehrabian: *Mater. Sci. Eng.*, 1979, **40**, 105–110.
9. Z. P. Guo, S. M. Xiong, B. C. Liu, L. Mei and J. Allison: *Int. J. Heat Mass Transfer*, 2008, **51**, 6032–6038.
10. Z. P. Guo, S. M. Xiong, B. C. Liu, M. Li and J. Allison: *Metall. Mater. Trans. A*, 2008, **39A**, 2896–2905.
11. A. Hamasaiid, G. Dour, M. S. Dargusch, T. Loulou, C. Davidson and G. Savage: *Metall. Mater. Trans. A*, 2008, **39A**, 853–864.
12. J. V. Beck, B. Blackwell and C. R. S. Clair: 'Inverse heat conduction: ill-posed problems', 125–130; 1985, New York, Wiley-Interscience.
13. F. Michael, P. R. Louchez and F. H. Samuel: *AFS Trans.*, 1995, **103**, 275–283.
14. C. P. Hallam and W. D. Griffiths: *Metall. Mater. Trans. B*, 2004, **35B**, 721–733.
15. C. P. Hallam, W. D. Griffiths and N. D. Butler: *Mater. Sci. Forum*, 2000, **329–330**, 467–472.
16. S. Broucaret, A. Michrafy and G. Dour: *J. Mater. Process. Technol.*, 2001, **110**, 211–217.